3D UAV Navigation with Moving-Obstacle Avoidance Using Barrier Lyapunov Functions

Esteban Restrepo, Ioannis Sarras, Antonio Loria, Julien Marzat

3D UAV Navigation with Moving-Obstacle Avoidance Using Barrier Lyapunov Functions

Esteban Restrepo * **Ioannis Sarras** * **Antonio Loría** ** **Julien Marzat** *

* *DTIS, ONERA, Université Paris-Saclay, F-91123 Palaiseau, France (e-mail: {esteban.restrepo, ioannis.sarras, julien.marzat}@onera.fr).*
** *LSS-SUPELEC, CNRS, 91192 Gif-sur-Yvette, France, (e-mail: loria@lss.supelec.fr)*

Abstract: We address the safe-navigation problem for aerial robots in the presence of mobile obstacles. Our approach relies on an original dynamic model defined in a cylindrical-coordinate space. It is assumed that the environment contains moving obstacles, that are encoded as state constraints so that they are embedded in the control design: the controller is constructed so as to generate a force field which, in turn, is derived from a potential with negative gradient in the vicinity of stable equilibria and positive gradient in the vicinity of obstacles. In particular, we combine the so-called Barrier Lyapunov Functions (BLF) method with the backstepping technique to obtain a smooth time-invariant controller. It is guaranteed that the robot reaches its destination from any initial condition in the valid workspace (that is, the environment stripped of the obstacles' safety neighborhoods) while avoiding collisions. Furthermore, the performance of our control approach is illustrated via simulations and experiments on a quadrotor benchmark.

Keywords: Autonomous mobile robots, obstacle avoidance, nonholonomic system, nonlinear control, constrained systems, backstepping, barrier functions.

1. INTRODUCTION

Navigation of robotic vehicles in cluttered environments has been widely studied in the last decade and continues to be a subject of great interest, with a large number of different techniques available in the literature (Hoy et al. (2015)). One of the most commonly used methods for robot navigation among obstacles is the Artificial Potential Functions (APF) approach; it consists in building a potential field on the workspace where the goal creates an attractive force and the obstacles create repulsive ones. A few variations of this approach have been developed in the literature: *e.g.*, in Kim and Khosla (1992) harmonic potential functions are used in order to eliminate local minima, in Huang et al. (2006) artificial potential functions are used for obstacle avoidance of a nonholonomic vehicle by creating a potential function that affects the steering rather than the position, and in Guldner et al. (1995) and Guldner and Utkin (1995) sliding-mode control is used to follow the gradient of an artificial potential. However, one of the main limitations of the APF approach is the existence of local minima, that is, points of the workspace where the repulsive and attractive forces cancel out, thereby generating multiple equilibria. In addition to this, oscillations may appear in the proximity of obstacles that are close or in narrow passages, thereby causing collisions or even instability of the system.

Akin to the artificial potential functions, the navigation-functions (NF) method which was introduced in Rimon and Koditschek (1992) and further developed in Loizou (2011) and Loizou (2017), consists in transforming the workspace in which the robot and the obstacles are reduced to points via the so called *navigation transformation*. In this new space the control law can be designed as the negative gradient of the navigation function. Even though this method has been widely studied for the collision avoidance problem in environments with static obstacles and mainly in 2-dimensional workspaces, some extensions to the 3D navigation problem are laid, *e.g.*, in Loizou (2012) a navigation transformation is proposed for a topologically complex 3D workspace and in Roussos et al. (2008) this method is applied to a 3D nonholonomic vehicle. The NF-based approach is promising to guarantee the non-collision with multiple *static* obstacles, but the corresponding literature is mostly focused either on linear (or linearized) robot dynamics models, which are obviously not realistic let alone for 3D and UAV applications, or in nonholonomic vehicles with time-varying or discontinuous control laws. However, the former laws are generally difficult to design and analyze, while the latter are sensitive to measurement noise and challenging for stability analysis. Furthermore, their extension to the case of moving obstacles is not trivial.

A completely different viewpoint consists in regarding obstacles as state constraints on the robot. In this context, model predictive control (MPC) has been extremely popular for the navigation problem in cluttered environments since it allows to easily encode state and input constraints, see for example Park et al. (2009); Lee et al. (2011); Marzat et al. (2017). However, MPC can be computationally costly when accounting for multiple obstacles and nonlinear dy-

namics, and with unspecified stability margins. In this paper we use instead a more analytic approach: the so-called Barrier Lyapunov functions method (Tee et al. (2008)), to design a controller for autonomous vehicles evolving in 3D environments containing moving obstacles. Barrier Lyapunov functions allow to encode the obstacles as constraints on the system and directly use them as Lyapunov functions for the design of a stabilizing feedback law, thereby guaranteeing that the vehicle does not penetrate the constrained set and, consequently, ensuring navigation safety.

The contributions of this paper are twofold: firstly, we introduce a realistic 3D model based on distances and line-of-sight angles; it is important to stress that this model does not belong to the class of nonholonomic systems studied by Brockett (1983) for which there is an inherent impediment to design smooth time-invariant controllers. Then, we design a smooth controller that ensures the stabilization of any point in the valid workspace, that is, the environment space leaving out the obstacles neighborhoods. The rest of the paper is organized as follows: in Section 2 the control problem is formulated and our new model is presented, in Section 3 the feedback control scheme is presented and analyzed, in Section 4 simulation and experimental results demonstrating the efficiency of the proposed method are presented. Finally, some conclusions and ideas on future research are summarized in Section 5.

2. SYSTEM AND PROBLEM STATEMENT

2.1 3D nonholonomic model

Let us consider a 3-dimensional unmanned aerial vehicle with Cartesian position determined by the coordinates x, y, and z. Then, neglecting roll-orientation, the vehicle's motion is described by the following equations:

$$\dot{x} = v\cos\theta\cos\psi \tag{1a}$$
$$\dot{y} = v\cos\theta\sin\psi \tag{1b}$$
$$\dot{z} = -v\sin\theta \tag{1c}$$
$$\dot{\theta} = q \tag{1d}$$
$$\dot{\psi} = \frac{r}{\cos\theta} \tag{1e}$$

where v is the linear velocity, θ and ψ are the *pitch* and *yaw* angles, and q and r are the associated angular velocities.

The system (1) belongs to the class of driftless systems that are not stabilizable to a set-point via smooth time-invariant feedback (Brockett (1983)). This fact adds considerable complexity to the problem of navigation of the 3D nonholonomic vehicles, all the more in the presence of state constraints, such as those imposed by the presence of obstacles in the environment. Motivated by this limitation, we propose an alternative model that is inspired by Aicardi et al. (1995) where a transformation of a 2D unicycle model into polar coordinates is used. In 3D, the resulting model, which is equivalent to (1a)-(1e), is expressed in cylindrical coordinates with respect to the target point:

$$\dot{\rho} = -v\cos\alpha\cos\theta \tag{2a}$$
$$\dot{\beta} = \frac{v}{\rho}\sin\alpha\cos\theta \tag{2b}$$
$$\dot{z} = -v\sin\theta \tag{2c}$$
$$\dot{\alpha} = \frac{v}{\rho}\sin\alpha\cos\theta - \omega_1 \tag{2d}$$
$$\dot{\theta} = \omega_2 \tag{2e}$$

where $\rho := \sqrt{(x_g - x)^2 + (y_g - y)^2}$ is the distance to the goal position (x_g, y_g) in the XY plane, $\alpha := \text{atan2}(y_g - y, x_g - x) - \psi$ is the angle between the robot's body frame and the line-of-sight to the the goal in the XY plane, $\beta := \alpha + \psi$ is its angular position in the XY plane as seen from the goal coordinate system, and the angular inputs defined as $\omega_1 := r/\cos\theta$ and $\omega_2 := q$.

The model (2) does *not* belong to the class of driftless systems for which, according to Brockett (1983), the origin cannot be stabilized using smooth time-invariant feedback. However, the system's equations are not defined at the limit point $\rho = 0$, but this may be handled via feedback. From a practical viewpoint, a clear advantage of the model (2) is that it is more suitable for control implementation since, it is expressed in terms of the most often measured variables: distances and line-of-sight angles.

2.2 Problem statement

Consider a workspace $\mathcal{W} \subset \mathbb{R}^3$ with m static or moving obstacles with positions (x_{oi}, y_{oi}, z_{oi}) in the Earth reference frame and velocities $\eta_{oi} := [\dot{x}_{oi}, \dot{y}_{oi}, \dot{z}_{oi}]$ hence, with $i \leq m$. Let R_i denote the radius of a safety spherical zone completely covering the ith obstacle. The constrained-navigation problem consists in designing a control law that asymptotically steers the vehicle's posture to a desired configuration while staying away from each obstacle. More precisely, it is required to stabilize the origin $\{\rho = \beta = z = \alpha = \theta = 0\}$ while satisfying the constraints that $h_i(\rho, \beta, z) > 0$ for all $i \leq m$, where

$$h_i(\rho,\beta,z) := (\rho\cos\beta + x_{oi})^2 + (\rho\sin\beta + y_{oi})^2 + (z - z_{oi})^2 - R_i^2.$$

Remark 1. Note that $h_i = 0$ means that the vehicle is in contact with the ith obstacle's safety boundary.

3. CONTROL DESIGN

The navigation controller that we propose primarily relies on the observation that the system (2) has a natural *cascaded* structure: in the equations (2a)–(2c), we may regard α and θ as virtual control inputs so that, if we define control laws α^* and θ^* that steer ρ, β, and z to the origin, it would only be left to design the control laws ω_1 and ω_2 to make $\alpha \to \alpha^*$ and $\theta \to \theta^*$. This reasoning is at the basis of the well-known backstepping control method (Krstić et al. (1995)) but, while it is intuitively simple, it requires a careful handling in the realm of nonlinear systems. Here, we follow the same reasoning used in (Panteley and Loria, 2001, Proof of Lemma 2): for cascaded systems of the form

$$\dot{x}_1 = f_1(t, x_1) + g(t, x)x_2 \tag{3a}$$
$$\dot{x}_2 = f_2(t, x_2), \tag{3b}$$

where asymptotic stability of the origin can be demonstrated by showing the asymptotic stability of the nominal systems $\dot{x}_1 = f_1(t, x_1)$ and $\dot{x}_2 = f_2(t, x_2)$ and boundedness of the solutions of (3).

Thus, the controller is crafted with the aim at having the closed-loop system in a cascaded structure, with states $x_1 := [\rho, \beta, z]^\top$ and $x_2 := \left[\tilde{\alpha}, \tilde{\theta}\right]^\top$ where $\tilde{\alpha} := \alpha - \alpha^*$ and $\tilde{\theta} := \theta - \theta^*$. In these coordinates, the system (2) is equivalently written as

$$\begin{aligned}\dot{\rho} =& - v\cos\alpha^*\cos(\theta^*)\\ &+ v\left[\cos\alpha^*\cos\theta^* - \cos(\tilde{\alpha}+\alpha^*)\cos(\tilde{\theta}+\theta^*)\right] \qquad (4a)\\ \dot{\beta} =& \frac{v}{\rho}\sin\alpha^*\cos\theta^*\\ &+ \frac{v}{\rho}\left[\sin(\tilde{\alpha}+\alpha^*)\cos(\tilde{\theta}+\theta^*) - \sin\alpha^*\cos\theta^*\right] \qquad (4b)\\ \dot{z} =& - v\sin\theta^* + v\left[\sin\theta^* - \sin(\tilde{\theta}+\theta^*)\right] \qquad (4c)\end{aligned}$$

$$\begin{aligned}\dot{\tilde{\alpha}} =& \frac{v}{\rho}\sin(\tilde{\alpha}+\alpha^*)\cos(\tilde{\theta}+\theta^*) - \omega_1 - \dot{\alpha}^* \qquad (5a)\\ \dot{\tilde{\theta}} =& \omega_2 - \dot{\theta}^* \qquad (5b)\end{aligned}$$

where α^* and θ^* are yet to be defined. Then, for this system to have a cascaded structure, the controls ω_1 and ω_2 are set to

$$\begin{aligned}\omega_1 :=& k_\alpha\tilde{\alpha} + \frac{v}{\rho}\sin(\tilde{\alpha}+\alpha^*)\cos(\tilde{\theta}+\theta^*) - \dot{\alpha}^* \qquad (6)\\ \omega_2 :=& - k_\theta\tilde{\theta} + \dot{\theta}^* \qquad (7)\end{aligned}$$

where k_θ and $k_\alpha > 0$. Indeed, in this case the closed-loop equations become

$$\begin{aligned}\dot{x}_1 =& v\, f_1(x_1) + v\, g(x_1, x_2) \qquad (8)\\ \dot{x}_2 =& f_2(x_2) \qquad (9)\end{aligned}$$

where

$$f_1(x_1) = \left[-\cos\alpha^*\cos(\theta^*), \frac{1}{\rho}\sin\alpha^*\cos\theta^*, -\sin\theta^*\right]^\top, \qquad (10)$$

$$f_2(x_2) = -\mathbf{k}^\top x_2, \quad \mathbf{k} := [k_\alpha, k_\theta]^\top, \qquad (11)$$

and

$$g(x_1, x_2) = \begin{bmatrix} \cos\alpha^*\cos\theta^* - \cos(\tilde{\alpha}+\alpha^*)\cos(\tilde{\theta}+\theta^*) \\ \frac{1}{\rho}\left[\sin(\tilde{\alpha}+\alpha^*)\cos(\tilde{\theta}+\theta^*) - \sin\alpha^*\cos\theta^*\right] \\ \sin\theta^* - \sin(\tilde{\theta}+\theta^*) \end{bmatrix} \qquad (12)$$

As mentioned previously, it must be established that the respective nominal systems $\dot{x}_1 = vf_1(x_1)$ and $\dot{x}_2 = f_2(x_2)$ are asymptotically stable. For the latter, this is a trivial task: it may be verified using the function

$$V_2(\tilde{\alpha}, \tilde{\theta}) := \frac{1}{2}\tilde{\alpha}^2 + \frac{1}{2}\tilde{\theta}^2 \qquad (13)$$

whose time derivative along the trajectories of (11), yields

$$\dot{V}_2 = -k_\alpha\tilde{\alpha}^2 - k_\theta\tilde{\theta}^2, \quad \forall(\tilde{\alpha}, \tilde{\theta}) \neq 0. \qquad (14)$$

For the nominal dynamics $\dot{x}_1 = vf_1(x_1)$ we use a Lyapunov-based design with the so-called Barrier Lyapunov function. For the sake of clarity, we recall the following definition, taken from Tee et al. (2008).

Definition 1. A Barrier Lyapunov Function is a scalar function $B(x)$, defined with respect to the system $\dot{x} = f(x)$ on an open region $\mathcal{D}$ containing the origin, that is continuous, positive definite, has continuous first-order partial derivatives at every point of $\mathcal{D}$, has the property $B(x) \to \infty$ as x approaches the boundary of $\mathcal{D}$, and satisfies $B(x(t)) \leq b$ for all $t \geq 0$ where $x(t)$ corresponds to the solution of $\dot{x} = f(x)$ for $x(0) \in \mathcal{D}$ and some positive constant b.

To design a barrier Lyapunov function for our system we use the constraints $h_i > 0$ and define the function

$$B(\rho, \beta, z) := \frac{1}{2}\sum_{i=1}^{m}\ln\left(\frac{h_{oi}}{h_i(\rho, \beta, z)}\right)^2 \qquad (15)$$

where $h_{oi} := x_{oi}^2 + y_{oi}^2 + z_{oi}^2 - R_i^2$. $B(\rho, \beta, z)$ satisfies Definition 1 since it is positive definite for all ρ, β, z such that $h_i > 0$ and tends to $+\infty$ as any $h_i(\rho, \beta, z) \to 0$.

Considering the nominal part of subsystem (8), $\dot{x}_1 = v\, f_1(x_1)$, let us define the candidate Lyapunov function

$$V_1(\rho, \beta, z) := \quad c_1\left[\rho^2 + \beta^2 + z^2\right] + c_2 B(\rho, \beta, z) \qquad (16)$$

with tuning parameters $c_1,\ c_2 > 0$, and defined in the set $\mathcal{D} := \left\{(\rho, \beta, z) \in \mathbb{R}_{\geq 0} \times \mathbb{R} \times \mathbb{R}\,; i \leq m\ :\ h_i(\rho, \beta, z) > 0\right\}$. Let the inputs v, α^* and θ^* be defined as

$$\begin{aligned}v :=& k_\rho\bar{v} - \frac{1}{\zeta^\top f_1(x_1)}\sum_{i=1}^{m}\zeta_{oi}^\top\begin{bmatrix}\dot{x}_{oi}\\ \dot{y}_{oi}\\ \dot{z}_{oi}\end{bmatrix} \qquad (17)\\ \bar{v} :=& \tanh(\rho) + \tanh(z)^2 \qquad (18)\\ \alpha^* :=& \operatorname{atan2}\left(-\frac{\partial V_1}{\partial\beta}, \frac{\partial V_1}{\partial\rho}\right) \qquad (19)\\ \theta^* :=& \operatorname{atan2}\left(\frac{\partial V_1}{\partial z}, |\bar{\zeta}|\right) \qquad (20)\end{aligned}$$

where $k_\rho > 0$, $\bar{\zeta} := \left[\frac{\partial V_1}{\partial\rho},\ \frac{\partial V_1}{\partial\beta}\right]^\top$, $\zeta := \frac{\partial V_1}{\partial x_1}$, and

$$\zeta_{oi} := \left[\frac{\partial V_1}{\partial x_{oi}},\ \frac{\partial V_1}{\partial y_{oi}},\ \frac{\partial V_1}{\partial z_{oi}}\right]^\top.$$

Substituting the inputs (17)-(20) into (10) and knowing that $\cos(\operatorname{atan2}(y, x)) = \frac{x}{\sqrt{x^2+y^2}}$ and $\sin(\operatorname{atan2}(y, x)) = \frac{y}{\sqrt{x^2+y^2}}$ we obtain the closed-loop nominal system:

$$\dot{x}_1 = -\frac{v}{|\zeta|}\left[\frac{\partial V_1}{\partial\rho},\ \frac{1}{\rho}\frac{\partial V_1}{\partial\beta},\ \frac{\partial V_1}{\partial z}\right]^\top \qquad (21)$$

so the derivative of (16) along (21) yields

$$\begin{aligned}\dot{V}_1 &= v\zeta^\top f_1(x_1) + \sum_{i=1}^{m}\zeta_{oi}\begin{bmatrix}\dot{x}_{oi}\\ \dot{y}_{oi}\\ \dot{z}_{oi}\end{bmatrix}\\ &= -\frac{\bar{v}\,\zeta^\top}{|\zeta|}\left[\frac{\partial V_1}{\partial\rho},\ \frac{1}{\rho}\frac{\partial V_1}{\partial\beta},\ \frac{\partial V_1}{\partial z}\right]^\top \qquad (22)\\ &\leq -k_\rho\bar{v}\min\left\{1, \frac{1}{\rho}\right\}|\zeta|\end{aligned}$$

that is, $\dot{V}_1$ is negative semidefinite. Indeed, the right-hand side of (22) vanishes at the destination point $\rho = \beta = z = 0$, as well as at the points where ζ is equal to zero, where

$$\zeta = \begin{bmatrix} c_1\rho - 2c_2 \sum_{i=1}^{m} \ln\left(\frac{h_{oi}}{h_i(\rho,\beta,z)}\right)\left(\frac{\rho + x_{oi}\cos\beta + y_{oi}\sin\beta}{h_i(\rho,\beta,z)}\right) \\ c_1\beta - 2c_2 \sum_{i=1}^{m} \ln\left(\frac{h_{oi}}{h_i(\rho,\beta,z)}\right)\left(\frac{\rho(x_{oi}\sin\beta - y_{oi}\cos\beta)}{h_i(\rho,\beta,z)}\right) \\ c_1\, z + 2c_2 \sum_{i=1}^{m} \ln\left(\frac{h_{oi}}{h_i(\rho,\beta,z)}\right)\left(\frac{z - z_{oi}}{h_i(\rho,\beta,z)}\right) \end{bmatrix} \tag{23}$$

That is, in general, V_1 in (16) may have local minima at points of the workspace that are away from the destination point. These may be avoided by properly tuning the parameter c_1 to sufficiently large values with respect to c_2 so that V_1 vanishes only at the origin and at finite number of disjoint unstable equilibrium points, one for each obstacle. Then V_1 has a unique minimum at the origin and $\dot{V}_1$ is negative everywhere except at the origin and a countable number of unstable equilibria. Asymptotic stability of the origin follows.

Remark 2. Note that, in view of (19) and (20), the controls defined in (6), (7) are equivalent to

$$\omega_1 = k_\alpha\tilde{\alpha} + \frac{v}{\rho}\sin(\tilde{\alpha}+\alpha^*)\cos(\tilde{\theta}+\theta^*) - \frac{1}{|\bar{\zeta}|^2}\left[\frac{\partial V_1}{\partial\beta}\frac{d}{dt}\left(\frac{\partial V_1}{\partial\rho}\right) - \frac{\partial V_1}{\partial\rho}\frac{d}{dt}\left(\frac{\partial V_1}{\partial\beta}\right)\right] \tag{24}$$

$$\omega_2 = -k_\theta\tilde{\theta} + \frac{1}{|\zeta|^2}\left[|\bar{\zeta}|\frac{d}{dt}\left(\frac{\partial V_1}{\partial z}\right) - \frac{\partial V_1}{\partial z}\frac{d|\bar{\zeta}|}{dt}\right] \tag{25}$$

when $\rho \neq 0$ and $\omega_1 = \omega_2 = 0$ when $\rho = 0$.

Now, the main result of this paper can be presented in the form of the following proposition.

Proposition 1. The error system (8)-(11) in closed-loop with the feedback law (17), (24), (25) is asymptotically stable at the origin in $\mathcal{D} := \{(\rho,\beta,z) \in \mathbb{R}_{\geq 0} \times \mathbb{R} \times \mathbb{R}\,; i \leq m : h_i(\rho,\beta,z) > 0\}$ and solves the safe navigation problem in a workspace $\mathcal{W}$ with m static/mobile obstacles.

Proof. As explained above, the statement follows the same reasoning used in (Panteley and Loria, 2001, Proof of Lemma 2) for cascaded systems of the form (8)-(11). For such systems, asymptotic stability of the origin can be demonstrated by showing the asymptotic stability of the nominal systems $\dot{x}_1 = v\ f_1(x_1)$ and $\dot{x}_2 = f_2(x_2)$ and boundedness of the solutions of (8)-(11). Asymptotic stability of the nominal subsystems $\dot{x}_1 = v\ f_1(x_1)$ and $\dot{x}_2 = f_2(x_2)$ was shown above. Moreover, for the solutions of the latter, we have $|x_2(t)| \leq \nu(t,t_0,x_{20})$ where $\nu(t,t_0,x_{20}) := \kappa|x_2(t_0)|\mathrm{e}^{-\lambda(t-t_0)}$.

Now, let us consider the subsystem (8) and the Lyapunov function (16). The derivative of V_1 along the solutions of (8) with inputs (17)-(20) yields:

$$\dot{V}_1 \leq -k_\rho\bar{v}\min\left\{1,\frac{1}{\rho}\right\}|\zeta| + \left[k_\rho\bar{v} + \frac{1}{|\zeta||f_1(x_1)|}\sum_{i=1}^{m}|\zeta_{oi}||\eta_{oi}|\right]|\zeta|\begin{bmatrix}\gamma_1(|x_2|)\\ \frac{1}{\rho}\gamma_2(|x_2|)\\ |\tilde{\theta}|\end{bmatrix} \tag{26}$$

where we used the fact that $g(x_1,x_2)$ is Lipschitz –see (12), and where $\gamma_1(s)$, $\gamma_2(s)$ are proportional to s.

In order to show boundedness of the solutions of (8) we proceed by contradiction: if $|x_1| \gg 1$ we have $\min\left\{1,\frac{1}{\rho}\right\} = \frac{1}{\rho}$ and $\bar{v}$ saturates —see (18). Furthermore, since the term $\frac{1}{|\zeta||f_1(x_1)|}\sum_{i=1}^{m}|\zeta_{oi}||\eta_{oi}|$ is bounded (see Appendix A) we may rewrite (26) as follows:

$$\dot{V}_1(t,x_1) \leq -k_\rho b_1\frac{|\zeta|}{\rho} + [k_\rho b_2 + b_3]\frac{|\zeta|}{\rho}|x_2| \tag{27}$$

where b_1, b_2, b_3 are positive constants. From (14) we showed that x_2 tends exponentially to zero, therefore the $\dot{V}_1$ can be bounded as

$$\dot{V}_1(t,x_1(t)) \leq -\frac{k_\rho}{\rho}|\zeta|\big[b_1 - b_4\nu(t,t_0,x_{20})\big] \tag{28}$$

where $b_4 := (k_\rho b_2 + b_3)$. From (28) it follows that $\dot{V}_1 \leq 0$ for sufficiently large t and, since V_1 is radially unbounded with respect to x_1, we conclude that the solutions of (8) are bounded and therefore the origin of system (8)-(11) is asymptotically stable in $\mathcal{D}$ except in a set of measure zero of unstable equilibria.

4. SIMULATION AND EXPERIMENTAL RESULTS

4.1 Simulations

To demonstrate the efficiency of the proposed control law (17), (24) and (25) for the stabilization of the origin, we consider a simulation example where a drone evolves in the presence of three mobile obstacles. In this scenario the objective is to steer the vehicle from the initial configuration $(x(0),y(0),z(0),\theta(0),\psi(0)) = (-3,-6,-3,0,0)$ to the origin avoiding the obstacles in the workspace. Controller parameters were chosen as $k_\rho = k_\alpha = 1$, $k_\theta = 3$, $c_1 = 1$ and $c_2 = 0.25$. Fig. 1 depicts the simulated workspace where the obstacles are represented by the colored spheres, with trajectories in red, and the blue crosses represent the trajectory described by the robot. The simulation results are depicted in Fig. 1-Fig. 4. In particular, Fig. 2 shows the distance between the vehicle and the obstacles for the duration of the simulation, which leads to conclude that the UAV successfully avoids the possible collisions in its path to the goal. Figures 3-4 show the evolution of the state which asymptotically approaches the origin, in accordance with the previous analysis.

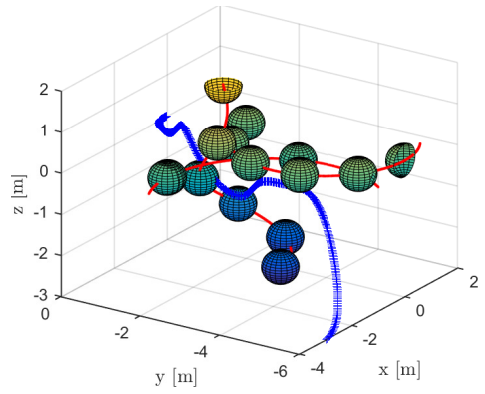

Fig. 1. Moving obstacles simulation – Vehicle's motion

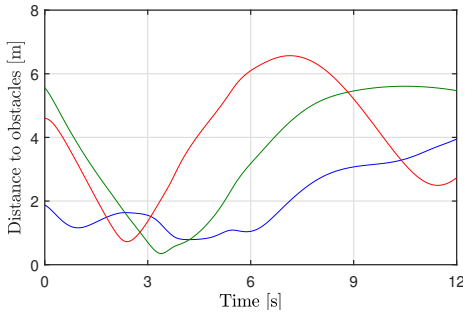

Fig. 2. Moving obstacles simulation – Distance to obstacles

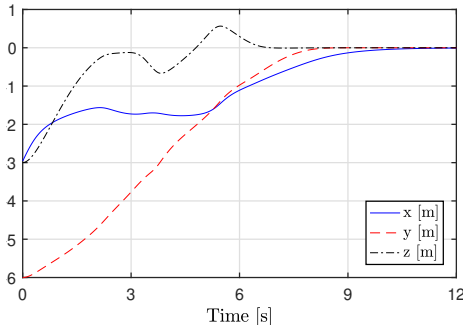

Fig. 3. Moving obstacles simulation – Cartesian position

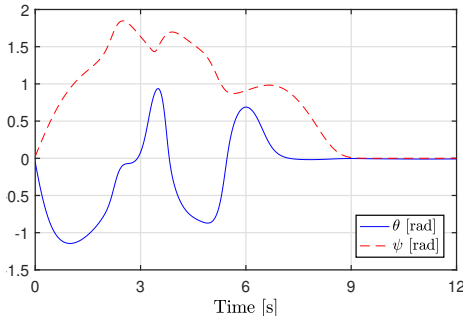

Fig. 4. Moving obstacles simulation – Orientation

4.2 Experimental Results

To further validate our results, some experiments were performed with one of the drones available at ONERA-Palaiseau, France. For the setup we used a Parrot AR.Drone and the Robot Operating System (ROS) interface for the implementation of the control law. An Optitrack motion capture system based on active IR cameras and markers was used to obtain the robot configuration at all time. Furthermore, odometry from the robot's sensors and the motion capture system also allowed us to obtain the linear and angular velocities of the vehicle with a reduced noise level. Two results are presented; in the first case (Fig. 5), the goal is to steer the robot to the final configuration $(x, y, z, \theta, \psi) = (1.6, 1.7, 1, 0, \pi/2)$ and in the second one (Fig. 7) the vehicle is to arrive to $(x, y, z, \theta, \psi) = (2, 2, 1, 0, 0)$. In both cases the initial configuration is set to $(x, y, z, \theta, \psi) = (-1.9, -0.48, 0.9, 0, \pi/2)$

Figures 5 and 7 illustrate the workspaces used for the experiments. The blue crosses represent the path performed by the actual drone. For both cases two virtual mobile obstacles, represented by colored spheres, with motions described by a 3-dimensional nonholonomic model as in (1) were made to follow circular paths (illustrated in red) at a constant altitude in the path between the drone's initial position and the target position; in the first experiment both obstacles move with a linear velocity of 0.3 m/s and a *yaw* rate of 0.65 rad/s; in the second experiment linear velocity and *yaw* rate were increased to 0.5 m/s and 1 rad/s respectively. As it may be appreciated from Figures 6 and 8, the distances to the obstacles remain bounded away from zero implying that the robot successfully navigates through the environment avoiding collisions with the mobile obstacles, as was expected from the theoretical results.

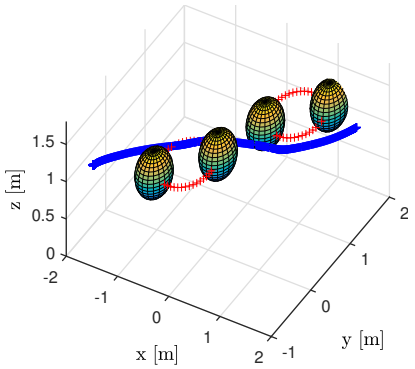

Fig. 5. Experiment 1 – Vehicle's motion

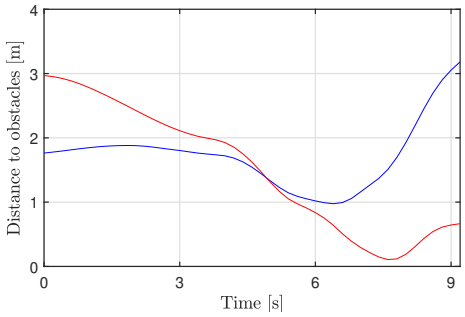

Fig. 6. Experiment 1 – Distance to obstacles

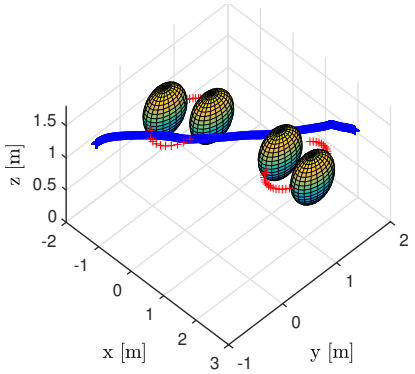

Fig. 7. Experiment 2 – Vehicle's motion

5. CONCLUSION

We have presented a feedback law for the navigation and obstacle avoidance of a 3D UAV using the concept of Barrier Lyapunov functions. This procedure allows us to

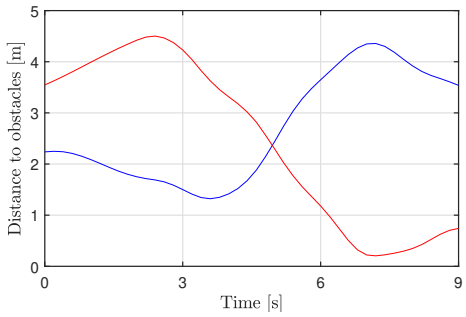

Fig. 8. Experiment 2 – Distance to obstacles

explicitly include the state constraints imposed by the obstacle avoidance requirement into the design of the control law and at the same time ensure asymptotic stability of the goal through a classical Lyapunov analysis. Moreover by transforming the nonholonomic model using cylindrical coordinates we are able to use a simpler smooth time-invariant feedback law for the stabilization of the origin. These results have been validated through simulations and some experiments. Further research includes the construction of a tuning-free Lyapunov Barrier function for encoding the state constraints as well as extensive experiments. Other possible extensions will consider realistic constraints such as input saturation and field-of-view constraints.

REFERENCES

Aicardi, M., Casalino, G., Bicchi, A., and Balestrino, A. (1995). Closed loop steering of unicycle like vehicles via Lyapunov techniques. *IEEE Robotics and Automation Magazine*, 2(4), 27 – 35.

Brockett, R.W. (1983). Asymptotic stability and feedback stabilization. In *Differential Geometric Control Theory*, 181 – 191. Birkhauser.

Guldner, J. and Utkin, V.I. (1995). Sliding mode control for gradient tracking and robot navigation using artificial potential fields. *IEEE Transactions on Robotics and Automation*, 11(2), 247–254.

Guldner, J., Utkin, V.I., Hashimoto, H., and Harashima, F. (1995). Tracking gradients of artificial potential fields with non-holonomic mobile robots. In *Proceedings of the American Control Conference*, volume 4, 2803–2804.

Hoy, M., Matveev, A.S., and Savkin, A.V. (2015). Algorithms for collision-free navigation of mobile robots in complex cluttered environments: a survey. *Robotica*, 33(3), 463497.

Huang, W.H., Fajen, B.R., Fink, J.R., and Warren, W.H. (2006). Visual navigation and obstacle avoidance using a steering potential function. *Robotics and Autonomous Systems*, 54(4), 288 – 299.

Kim, J.O. and Khosla, P.K. (1992). Real-time obstacle avoidance using harmonic potential functions. *IEEE Transactions on Robotics and Automation*, 8(3), 338–349.

Krstić, M., Kanellakopoulos, I., and Kokotović, P. (1995). *Nonlinear and adaptive control design*. Adaptive and learning systems for signal processing, communications, and control. Wiley.

Lee, D., Lim, H., and Kim, H.J. (2011). Obstacle avoidance using image-based visual servoing integrated with nonlinear model predictive control. In *Proceedings of the 50th IEEE Conference on Decision and Control and European Control Conference*, 5689–5694.

Loizou, S.G. (2011). Closed form navigation functions based on harmonic potentials. In *Proceedings of the 50th IEEE Conference on Decision and Control and European Control Conference*, 6361–6366.

Loizou, S.G. (2012). Navigation functions in topologically complex 3-d workspaces. In *2012 American Control Conference (ACC)*, 4861–4866.

Loizou, S.G. (2017). The navigation transformation. *IEEE Transactions on Robotics*, 33(6), 1516–1523.

Marzat, J., Bertrand, S., Eudes, A., Sanfourche, M., and Moras, J. (2017). Reactive MPC for autonomous MAV navigation in indoor cluttered environments: Flight experiments. *IFAC-PapersOnLine*, 50(1), 15996 – 16002. 20th IFAC World Congress.

Panteley, E. and Loria, A. (2001). Growth rate conditions for uniform asymptotic stability of cascaded time-varying systems. *Automatica*, 37(3), 453 – 460.

Park, J.M., Kim, D.W., Yoon, Y.S., Kim, H.J., and Yi, K.S. (2009). Obstacle avoidance of autonomous vehicles based on model predictive control. *Proceedings of the Institution of Mechanical Engineers, Part D: Journal of Automobile Engineering*, 223(12), 1499–1516.

Rimon, E. and Koditschek, D.E. (1992). Exact robot navigation using artificial potential functions. *IEEE Transactions on Robotics and Automation*, 8(5), 501–518.

Roussos, G.P., Dimarogonas, D.V., and Kyriakopoulos, K.J. (2008). 3d navigation and collision avoidance for a non-holonomic vehicle. In *2008 American Control Conference*, 3512–3517.

Tee, K.P., Ge, S.S., and Tay, E.H. (2008). Barrier Lyapunov Functions for the control of output-constrained nonlinear systems. *Automatica*, 45(4), 918–927.

Appendix A

The explicit expressions of the gradient of V_1 with respect to x_1 and with respect to the coordinates of the obstacles, respectively ζ and ζ_{oi} are given in (23) and

$$\zeta_{oi} = \begin{bmatrix} 2c_2 \sum_{i=1}^{m} \ln\left(\frac{h_{oi}}{h_i(\rho,\beta,z)}\right)\left(\frac{x_{oi}}{h_{oi}} - \frac{\rho\cos\beta + x_{oi}}{h_i(\rho,\beta,z)}\right) \\ 2c_2 \sum_{i=1}^{m} \ln\left(\frac{h_{oi}}{h_i(\rho,\beta,z)}\right)\left(\frac{y_{oi}}{h_{oi}} - \frac{\rho\sin\beta + y_{oi}}{h_i(\rho,\beta,z)}\right) \\ 2c_2 \sum_{i=1}^{m} \ln\left(\frac{h_{oi}}{h_i(\rho,\beta,z)}\right)\left(\frac{z_{oi}}{h_{oi}} + \frac{z - z_{oi}}{h_i(\rho,\beta,z)}\right) \end{bmatrix}$$

and it can be seen that both functions can be bounded by expressions of the form

$$\left|\frac{\partial V_1}{\partial x_1}\right| \leq k_1|x_1| + k_2|\ln(h_i)|$$

$$\left|\frac{\partial V_1}{\partial w_{oi}}\right| \leq k_1' + k_2'|\ln(h_i)| \quad w_{oi} := x_{oi}, y_{oi}, z_{oi}$$

and therefore, since $|\zeta|$ and $|\zeta_{oi}|$ are of the same order of magnitude, $|\zeta_{oi}|/|\zeta|$ can be upper bounded by a constant. Moreover, since $|\eta_{oi}|$ is bounded and, from (28), it follows that $|f_1(x_1(t))|$ is bounded, we may conclude that the expression $\frac{1}{|\zeta||f_1(x_1)|}\sum_{i=1}^{m}|\zeta_{oi}||\eta_{oi}|$ is also upper bounded by a constant.